NiO Nanoparticles Dispersed in Mesoporous Silica Glass

Nathália M. Carneiro,[†] Wallace C. Nunes,[‡] Rui P. Borges,[§] Margarida Godinho,[||] Luis E. Fernandez-Outon,[⊥] Waldemar A. A. Macedo,[⊥] and Italo O. Mazali*,[†]

Instituto de Química, Universidade Estadual de Campinas—UNICAMP, 13084-971, Campinas, SP, Brazil, Instituto de Física, Universidade Federal Fluminense—UFF, 24210-346 Niterói, RJ, Brazil, Centro de Física da Matéria Condensada da Universidade de Lisboa, Campo Grande, Ed. C8, 1749-016 Lisboa, Portugal, Departamento de Física, Faculdade de Ciências, Universidade de Lisboa, Campo Grande, Ed. C8, 1749-016 Lisboa, Portugal, and Serviço de Nanotecnologia, Centro de Desenvolvimento da Tecnologia Nuclear, 31270-901 Belo Horizonte, MG, Brazil

Received: May 21, 2010; Revised Manuscript Received: October 1, 2010

We have studied the magnetic properties of NiO nanoparticles dispersed into mesoporous silica glass with three particle size distributions obtained using the bottom-up nanofabrication technique. The samples were characterized by XRD, Raman, and TEM and found to consist of monodispersed rock salt structure NiO nanoparticles. The magnetic results indicate that the particles can be considered as an antiferromagnetically ordered core with an uncompensated magnetic moment, and a magnetically disordered surface. The magnetization loops exhibit a loop shift with intriguing temperature dependence. Furthermore, an increase in the average blocking temperature is observed with increases in the number of impregnation−decomposition cycles. These results are discussed considering the influence of the magnetic interaction on the core−shell structure of the nanoparticles.

Introduction

Magnetic nanoparticle (NP) systems have received considerable interest in recent years owing to their unique magnetic properties as well as their technological applications.[1−3] Magnetic nanoparticles show new properties or properties that are modified relative to those of bulk materials. The reduction of particle size to nanoscale levels leads to a complex interplay between finite size effects and surface effects, which is responsible for the magnetic behavior of nanoparticle magnetic systems.[1] Finite size effects are related to the reduced number of exchange-coupled spins within the particle. Surface effects are related to the reduced symmetry of surface atoms which have a nearest neighbor on one side and none on the other side, resulting in a larger number of broken exchange bonds and consequently surface anisotropy, magnetic frustration, and spin disorder. These effects are enhanced in antiferromagnetic (AF) nanoparticles due to the much lower core moment with respect to ferromagnetic (F) nanoparticles of the same size. According to the Néel model, nanoparticles of AF materials can have a net magnetic moment due to an uncompensated spin number in the two sublattices, depending on the crystal structure.[4] However, experiments on NiO AF nanoparticles have shown that the two-sublattice model cannot account for anomalous magnetic properties, such as large coercivities (H_C), field shifts of the hysteresis loop (H_E),[5] superparamagnetism, and spin-glass (SG) behaviors,[6] all of which are strongly particle-size-dependent.

Both theoretical and experimental published data on NiO nanoparticles show that the magnetic structure within the nanoparticle can differ strongly with respect to the bulk magnetic structure because of the influence of finite size and surface effects.[5−8] However, there is still some debate regarding the origin of such effects.[2] For instance, while the exchange bias effect can be demonstrated by considering a complex magnetic structure with as many as eight sublattices, some SG-like properties at low temperature are compatible with a core−shell structure, where a ferromagnetic or spin-disordered shell is exchange-coupled to an ordered AF core.[6,7]

In this work, we present an investigation of the effects of magnetic interparticle interactions and particle size distributions on the magnetic properties of NiO NPs dispersed into porous Vycor glass (PVG). The results obtained for zero-field-cooled (ZFC) and field-cooled (FC) magnetization, H_C and H_E, are interpreted on the basis of a core−shell structure, with an antiferromagnetic core and a disordered nonergodic shell. Our results suggest that interparticle interactions and particle size distribution of NiO NPs play an important role in H_C and H_E.

Experimental Methods

Mesoporous Silica Glass. The mesoporous silica glass utilized in this work was porous Vycor glass (PVG), code 7930, purchased from Corning Glass Company. The PVG was cleaned and activated as described by the manufacturer.[9]

Synthesis of NiO Nanoparticles Dispersed in Mesoporous Silica Glass. The precursor of the nickel oxide is the single-source metallo-organic compound nickel(II) 2-ethylhexanoate, $Ni[OOCCH(C_2H_5)C_4H_9]_2$, hereafter indicated as $Ni(hex)_2$, synthesized by a metathesis reaction.[10] This preparation is carried out by mixing 10.2644 g (0.06 mol) of anhydrous nickel acetate with 18.4327 g (0.12 mol) of 2-ethylhexanoic acid in a 250 mL round-bottom flask. It was stirred and heated under vacuum at 363 K for 4−5 h. The byproduct acetic acid was removed, and a clear green viscous liquid was obtained. The nanocomposites were prepared by impregnation of monoliths of PVG

* To whom correspondence should be addressed. Phone: +55-19-3521-3164. Fax: +55-19-3521-3023. E-mail address: mazali@iqm.unicamp.br.
[†] Universidade Estadual de Campinas—UNICAMP.
[‡] Universidade Federal Fluminense—UFF.
[§] Centro de Física da Matéria Condensada da Universidade de Lisboa.
[||] Faculdade de Ciências, Universidade de Lisboa.
[⊥] Centro de Desenvolvimento da Tecnologia Nuclear.

10.1021/jp1046886
Published on Web 10/15/2010

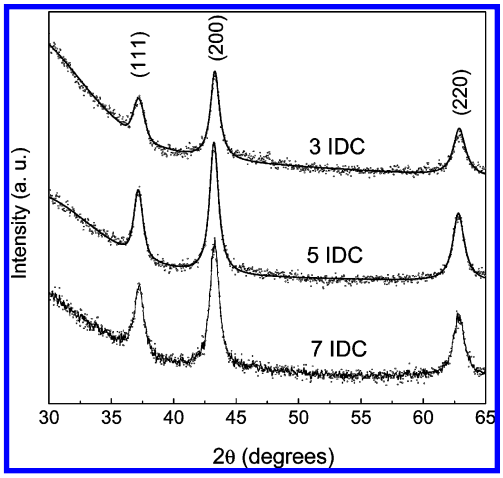

Figure 1. X-ray diffraction patterns for NiO NPs with three, five, and seven IDCs.

by a hexane solution of $Ni(hex)_2$ (0.8 mol L^{-1}) for 8 h, followed by a thermal treatment at 873 K for 8 h under a synthetic air flow. Nanocomposites of NiO in PVG with different particle size distributions were obtained by employing sequences of impregnation−decomposition cycles (IDCs).[7] We have prepared samples with three, five, and seven IDCs. All the monoliths, independent of the number of IDCs, were submitted to 7 thermal treatments, completing a total of 56 h at 873 K.

Characterizations. X-ray measurements were performed on a Shimadzu XRD-6000 powder diffractometer with CuKα radiation, in the step scan mode (0.01° with a 10 s counting time per step). Energy-filtered transmission electron microscopic (EFTEM) images were obtained using a Carl Zeiss CEM 902 microscope equipped with a Castaing−Henry energy filter spectrometer within the column and a Proscan Slow Scan charge-coupled device (CCD) camera, both controlled by a microcomputer running the AnaluSis 3.0 system. The magnetization measurements were performed in a superconducting quantum interference device (SQUID) magnetometer (Quantum Design MPMS).

Results and Discussion

X-ray powder diffraction patterns (Figure 1) showed well-defined peaks at 37.3°, 43.4°, and 63.0° (2θ) indicating the formation of the cubic phase of NiO (JCPDS file 00-047-1049). Below $2\theta = 40°$ the pattern is dominated by the large background signal coming from the noncrystalline PVG matrix. The IDC methodology showed a linear mass increment of the nanoparticles inside the PVG (data not shown) that is supposed to lead to an increase in the NiO crystallite size.[11] The variation of the crystallite size of the NiO nanoparticles as a function of the number of IDCs was evaluated from XRD (Figure 1) (using Scherrer's equation)[12] and EFTEM (Figure 2). The XRD diffraction patterns clearly show the increase of the intensity and a less pronounced decrease of the full-width at half-maximum (fwhm) with the increase in the number of IDCs. The crystallite size estimated from Scherrer's equation indicated an average crystallite size of 10 nm, independent of the number of IDC, probably due to the X-ray pattern being dominated by the large background signal coming from the noncrystallite PVG matrix below 40° (2θ).

The EFTEM images of samples obtained with three, five, and seven IDCs (Figure 2) show nearly spherical monodispersed NiO nanoparticles with particle size distributions dependent on the number of IDCs. The TEM dark field image of NiO/PVG

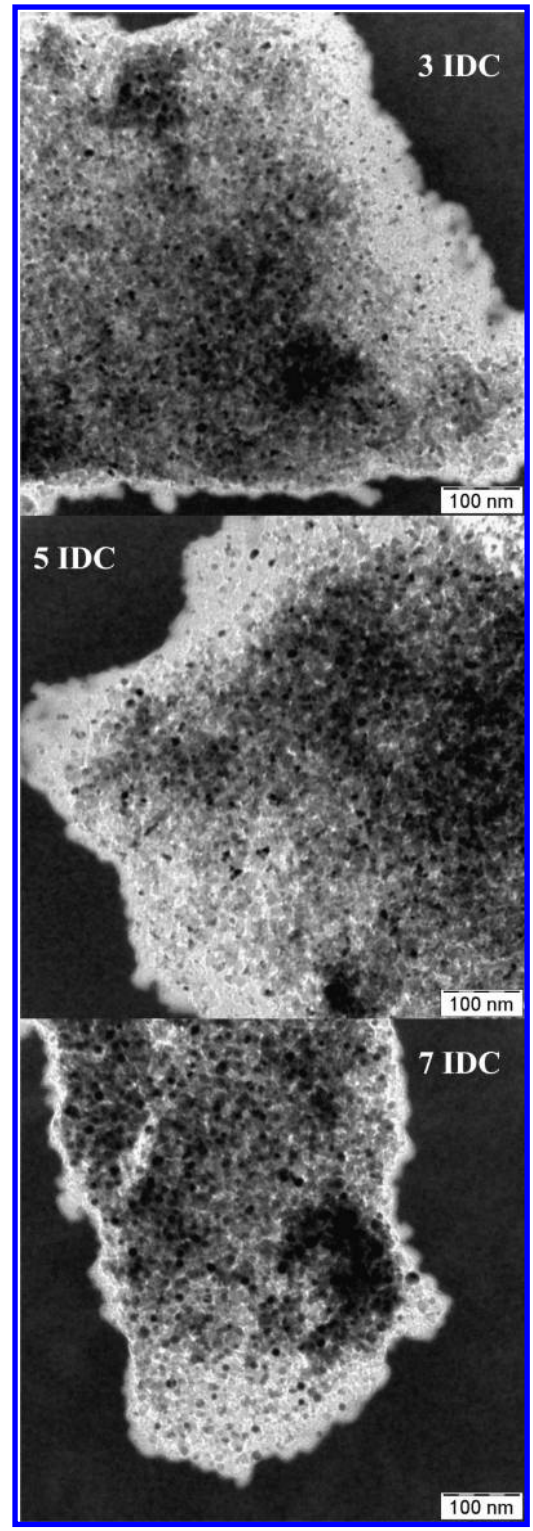

Figure 2. EFTEM images of NiO nanoparticles with three, five, and seven IDCs.

with seven IDCs (Figure 3) confirms the crystallinity of the NiO nanocrystals, in agreement with the X-ray data. The histogram of the particle size distributions and the variation of the average crystallite size with the number of IDCs are shown, respectively, in Figure 4a and 4b.

Figure 5 shows the ZFC and FC magnetization curves measured for different numbers of IDCs. By lowering the temperature, the FC curves show a continuous increase of magnetization value, and the ZFC curves show a broad maximum, followed by a small increase at low temperature.

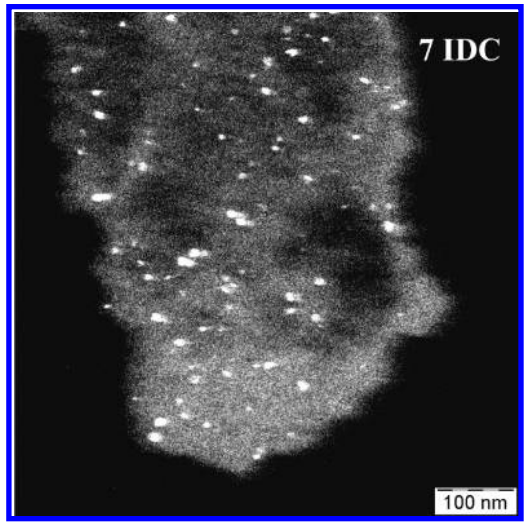

Figure 3. TEM dark field image of NiO NPs with seven IDCs, obtained using transmission electron microscopy.

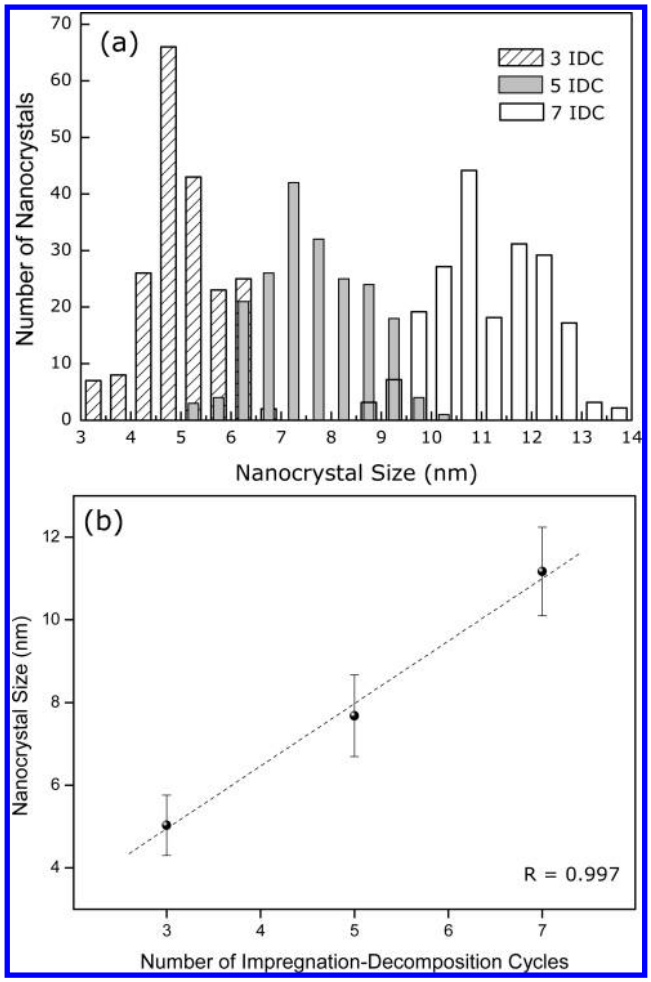

Figure 4. Histogram of the particle size distributions for different numbers of IDCs (a) and average nanocrystal size as a function of the number of impregnation−decomposition cycles for the PVG/NiO system (b).

As can be seen in Figure 5, the peak observed in the ZFC curves shifts to higher temperature with an increased number of IDCs, but the irreversibility temperatures determined by the separation between the ZFC and FC curves remain almost constant. The maximum in the ZFC curve is usually attributed to the average blocking temperature of the magnetic moment

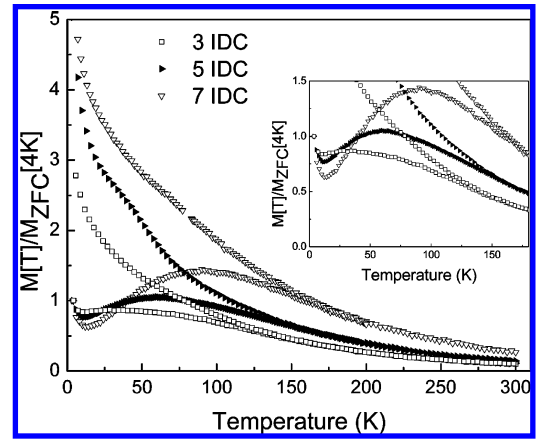

Figure 5. ZFC and FC magnetization curves of all samples studied. The inset shows the displacement to higher temperature of the maximum of ZFC curves by increasing the number of IDCs.

distribution, and the irreversibility temperature between the ZFC and FC curves corresponds to the largest energy barrier. Assuming that the measured magnetic moments are due to NiO uncompensated moments, the ZFC and FC curves can be described by considering a progressive blocking process of the core particle moment distribution. Moreover, experimental studies have suggested that the magnetic moment of NiO nanoparticles increases with their diameters.[13−15] Therefore, the observed increase of the peak temperature when increasing the number of IDCs can be ascribed to an increase of either the diameter or the anisotropy of the NPs.

Even though XRD measurements do not indicate large variations in the diameter of the particles with the IDC number, TEM grain size analysis shows that the median diameter increases from 5 to 7.5 to 11 nm for 3, 5, and 7 IDC cycles, respectively, as shown in Figure 4. Therefore the median volume of particles is an order of magnitude larger for the seven IDC set. It can be assumed that the reversal of the particles is due to thermal activation effects over distribution of energy barriers (ΔE). The relaxation over a single barrier for noninteracting particles with uniaxial anisotropy is described by the Néel−Arrhenius law given by

$$\tau^{-} = f_0 \exp[-\Delta E/k_B T]$$

where τ is the measurement time, f_0 is the attempt frequency for reversal, normally taken to be 10^9 s^{-1}, k_B is the Boltzmann constant, and T is the measurement temperature. Assuming a grain volume dependence of the energy barriers to reversal of the form, $\Delta E = K_{AF}V$, where K_{AF} is the magnetocrystalline anisotropy of the NiO particles and V is the median of the particle volume distribution for each IDC set based on TEM analysis, and a typical measurement time of 100 s, we obtain an expression of the form, $K_{AF}V = 25k_BT_B$, where T_B is the median blocking temperature. The values of T_B obtained from the maximum of the ZFC curves (Figure 5) are 36, 62, and 90 K (±5 K) for 3, 5, and 7 IDCs, respectively. The anisotropy constant calculated from this expression is $K_{AF}(T_B) \sim 1.89 \times 10^6$ erg/cm^3 for the 3 IDC set and 9.68×10^5 and 4.45×10^5 erg/cm^3 for the 5 and 7 IDC sets, showing a decrease in anisotropy with increasing IDC cycle number. Using the approximation that the AF moment, m_{AF}, is approximately $(T_N - T)^{1/3}$, and $K_{AF} \propto m_{AF}^3$ for uniaxial anisotropy, we obtain $K_{AF} = K_{AF}(0)[(T_N - T)/T_N]$ with $T_N \sim 520$ K.[16] Hence, the values of the anisotropy for the three sets at 293 K are 8.9×10^5, 4.8

$\times 10^5$, and 2.3×10^5 erg/cm^3 for the 3, 5, and 7 IDC sets. Therefore, the increase in the median blocking temperature with IDC cycling can be attributed to particle size effects. In order to do these calculations, we have assumed that the whole particle volume behaves as an AF core.

The value used for T_N in these calculations corresponds to bulk NiO. The exact value for thin films is expected to be lower as observed by Alders et al.[17] in epitaxial NiO ($a = 4.176$ Å) layers grown on MgO with different thicknesses. A reduced T_N would lead to further reduction in K_{AF}. Alders et al.[17] found that for 20, 10, and 5 monolayers, T_N is reduced to 470, 430, and 295 K, respectively. Hence, lower anisotropy values are expected for lower T_N. However, this does not significantly affect the argument exposed above. For instance, using these values as an estimate of T_N for the 5 IDC sample with median grain size of 7.5 nm, a decrease of about 12% would be expected for K_{AF}.

The increase of the blocking temperature could be associated with increasing magnetic interactions between the particles (due to the increase of particle concentration), as reported in other experimental and theoretical work.[14,18,19] However, the Vycor matrix excludes the possibility of magnetic exchange interaction between the NPs.[18−20] Also, the magnetic dipole interaction among AF NPs is usually negligible because the magnetic moments of AF NPs are typically much smaller than those of FM NPs. Therefore, insignificant effects of interparticle interactions are expected in the temperature range where the ZFC curves exhibit peaks.

As the particle size is reduced, the contribution of the shell is more pronounced. According to a core−shell description, a one atom thick shell would reduce the AF volume, which, in the case of the 3 IDC sample, would mean a 12% reduction in diameter and therefore a ~50% increase in anisotropy, while for a 11 nm particle K_{AF} would increase ~20%. However, as the particle diameters were measured by bright and dark field transmission electron microscopy, it is expected that the contribution of the shell atoms to the whole particle volume will not be appreciable on the measurement of the particle size from the TEM images due to local symmetry breaking of the lattice, broken bonds, and the defects characteristics of the shell structure. Some interesting magnetic effects associated with the shell have been observed below 25 K in NiO nanoparticles systems.[6,21,22] Discussion of such properties is based on a polycluster structure within the shell caused by surface effects. The disorder and competition of magnetic interactions between the small clusters within the shell can give rise to spin-glass freezing, i.e., a cooperative freezing of spins at a certain temperature below which a highly irreversibible, metastable frozen state occurs without the usual long-range spatial magnetic order.[23] For instance, spin-glass-like freezing at about 15 K was observed in a 3 nm NiO nanoparticles system.[4] Here we have observed a continuous increase of magnetization in ZFC and FC curves below 20 K for all samples studied. Such behavior is related to shell magnetization with probable freezing temperature below 20 K, since the mean particle sizes in our samples are rather bigger than 3 nm.

Therefore, in order to investigate magnetic properties associated with the shell in more detail, we have measured ZFC and FC hysteresis loops over a wide temperature range (2−180 K). Large coercivities and shifted hysteresis loops are observed for all samples after field cooling procedures. Figure 6 shows hysteresis loops measured at 10 K for the sample with 5 IDC for both ZFC and FC in 10 kOe from 300 K. As can be seen from the inset in Figure 6, the FC hysteresis loop is shifted

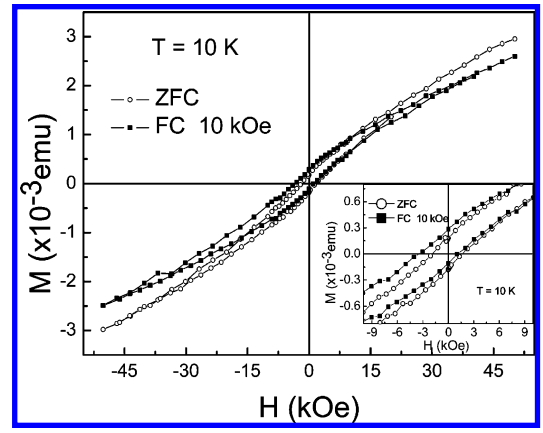

Figure 6. Magnetization vs applied field measured at a temperature of 10 K for both ZFC and FC from 300 K in 10 kOe. The inset is a close-up of the center of the hysteresis, showing the field shifts of the hysteresis.

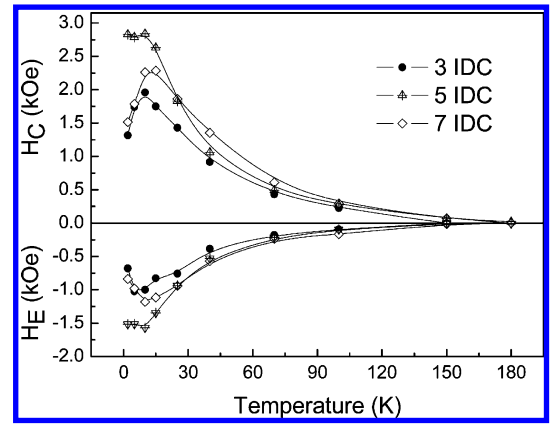

Figure 7. Evolution of the values of the field shift of hysteresis (H_E) and coercivity (H_C) with temperature, for all samples. The solid lines are guides for the eyes.

from the origin and broadened. The value of the field shift at 10 K is $H_E = -1.5$ kOe for the sample with 5 IDCs.

The temperature dependence of H_E and H_C was investigated in the temperature range 2−180 K for all samples and is shown in Figure 7. Both H_E and H_C go to zero at the irreversibility temperature for all samples. It is observed from Figure 7 that the change in the magnitude of H_E depends on both the number of IDCs and the temperature conditions.

Interestingly, for samples with 3 and 7 IDCs a maximum was observed at about 10 K for both H_E and H_C temperature variations. Although the observed temperature behavior of H_E is very similar to $H_C(T)$, the mechanisms responsible for such temperature dependences are different. The H_C temperature behavior can be understood considering the magnetic configuration within the NPs. With decreasing temperature, H_C increase until 10 ± 3 K is in agreement with what is expected for the progressive blocking process of core particle moments. The magnetization at this range of temperature, where most of the core particle moments are blocked, is mainly determined by the surface spins, which thermally fluctuate; i.e., it behaves like a paramagnetic contribution. With the subsequent decrease in temperature there is an increase of the paramagnetic contribution of the surface spins and clusters and, consequently, an actual narrowing of the hysteresis cycle. Similar H_C temperature behavior has been observed and described for FM NPs.[24,25] The sample with 5 IDCs does not exhibit a clear maximum at 10 K, probably due to the fact that, in this case, the paramagnetic type

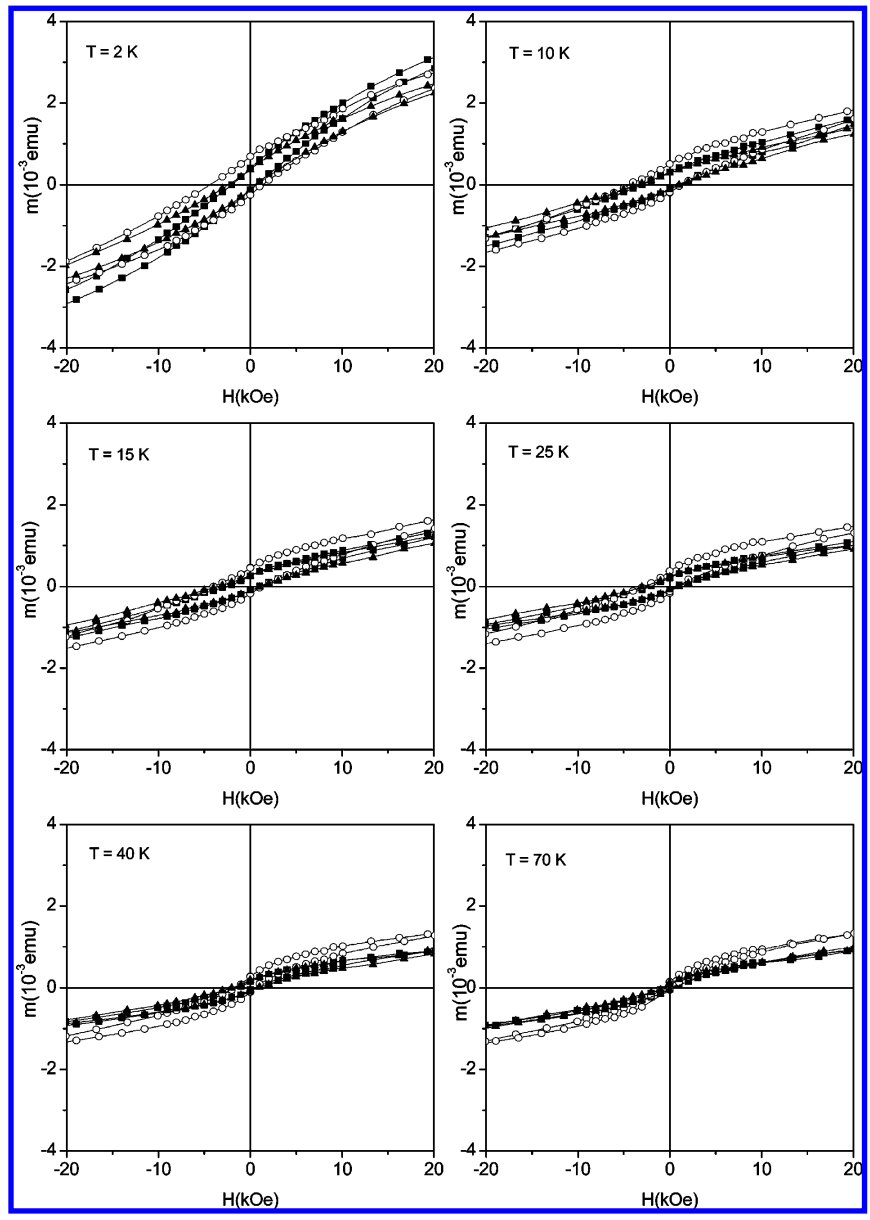

Figure 8. Close-up of the center of the hysteresis loops obtained for each sample: (■) 3 IDCs, (○) 5 IDCs, and (▲) 7 IDCs, at temperatures of 2, 10, 15, 25, 40, and 70 K.

contributions of the shell are not strong enough to dominate the magnetic behavior below 10 K.

On the other hand, the intriguing H_E temperature behavior may arise due to interface exchange coupling between the antiferromagnetically ordered core and the disordered shell clusters.[26,27] Above the irreversibility temperature between ZFC and FC curves, the core moments are in a superparamagnetic state, and, consequently, the H_E is zero. With decreasing temperature, the increase of H_E until around 10 K is in agreement with the progressive blocking process of the core moments. The subsequent decrease below 10 K, where most of the core nanoparticles are blocked, is mainly determined by the surface clusters. By decreasing the temperature, thermal fluctuations slow down and the magnetic correlation between clusters in the shell grows, leading to a low effective magnetic anisotropy of the shell clusters, and therefore is less effective to induce exchange bias; i.e., H_E decreases.

It is important to note that, although in the higher temperature range ($T > 25$ K) the H_E appears to increase with increasing number of IDCs, below 25 K we observe a decrease of the H_E when the number of IDCs increases from 5 to 7.

In order to have an insight into the possible mechanisms to explain the behavior of H_E at temperatures below 25 K for our samples, we have plotted the hysteresis loops at different temperatures. Figure 8 shows that below 25 K there is an increase in the slope of the M vs H hysteresis loops, indicating an increase in susceptibility that should contribute to reduction of H_E below 20 K. Below 25 K the three samples exhibit a sudden change in the trend of the temperature dependence of H_E (Figure 7), which appears to be compatible with a collective magnetic state typical of spin-glass-like behavior, probably F surface domains, demonstrating that below 20 K there is a fraction of surface spins which are strongly coupled by superexchange interactions.[21] The spin-glass-like behavior is also manifested as a sudden increase in susceptibility below a transition temperature, resulting in an enhancement of the uncompensated magnetic moment. This effect could be expected to decrease the value of the exchange field in a similar way as in the case of other exchange-biased systems for which an increase in the magnetization of the F layer results in the reduction of H_E.[28] It is notable that, in the case of the five IDCs curve, it experiences a less pronounced change in susceptibility

than the other two samples, which correlates with a lower decrease of H_E below the transition temperature.

However, given the nature of our samples, the number of IDC cycles increases the mass of NiO without leaving an option to weigh the exact mass of magnetic material contained in the sample due to the fact that the magnetic material is embedded in Vycor PVG glass matrix. From measurements of the initial mass susceptibility,[29] it would possible to estimate the average uncompensated moment in the sample and, assuming an average magnetic moment per Ni ion throughout the sample, the number of magnetic ions that correspond to that uncompensated moment may be obtained. Information about the unoxidized Ni content in the sample may help to discern the effects produced on the magnetic behavior by uncompensated moments whether due to uncompensated NiO moments or to Ni clusters. Since our XRD results shown in Figure 1 do not reflect any contribution from unoxided Ni, either crystalline or amorphous, in our samples, an eventual residual fraction of Ni clusters, ferromagnetic at low temperatures, will not affect in a significant manner our results. Nevertheless, experimental measurements of the portion of moments from NiO and Ni clusters would help in the interpretation of magnetic data and the development of theoretical models to explain the exchange bias behavior in NiO nanoparticles.

Conclusion

In conclusion, we have observed large coercivities and field-shifted hysteresis loops in NiO nanoparticles dispersed in Vycor glass for different numbers of impregnation−decomposition cycles. The experimental results suggest that the particle size and, consequently, the magnetic anisotropy are the main parameters that significantly change with the different numbers of IDCs. The coercivity and loop shift determined as a function of temperature display a maximum at about 10 K and a further decrease with increasing temperature approaching zero near the irreversibility temperature between the ZFC and FC curves. These observations are consistent with the core−shell magnetic configuration with FM clusters in the shell and an AF core.

Acknowledgment. The authors are grateful to FAPESP, FAPEMIG, CNPq, and CAPES for financial support and to Prof. C. H. Collins (IQ-UNICAMP, Brazil) for English revision. This is a contribution of the National Institute of Science and Technology in Complex Functional Materials (CNPp/MCT/Finep).

References and Notes

(1) Dormann, J. L.; Fiorani, D.; Tronc, E. *Adv. Chem. Phys.* **1997**, *98*, 283.
(2) Nogués, J.; Sort, J.; Langlais, V.; Skumryev, V.; Suriñach, S.; Muñoz, J. S.; Baró, M. D. *Phys. Rep.* **2005**, *422*, 65.
(3) Schneider, J. J. *Adv. Mater.* **2001**, *13*, 529.
(4) Néel, L. In *Low-Temperature Physics*; Dewitt, C., Dreyfus, B., deGennes, P. D., Eds.; Gordon and Breach: New York, 1962.
(5) Kodama, R. H. *J. Magn. Magn. Mater.* **1999**, *200*, 359.
(6) Winkler, E.; Zysler, R. D.; Mansilla, M. V.; Fiorani, D.; Rinaldi, D.; Vasilakaki, M.; Trohidou, K. N. *Nanotechnology* **2008**, *19*, 185702.
(7) Rubinstein, M.; Kodama, R. H.; Makhlouf, S. A. *J. Magn. Magn. Mater.* **2001**, *234*, 289.
(8) Bi, H.; Li, S.; Zhang, Y.; Du, Y. *J. Magn. Magn. Mater.* **2004**, *277*, 363.
(9) Available in www.corning.com/docs/specialtymaterials/pisheets/Vycor%207930.pdf.
(10) Vest, R. W.; Singaram, S. *Mater. Res. Soc. Symp. Proc.* **1986**, *60*, 35.
(11) Mazali, I. O.; Souza Filho, A. G.; Viana, B. C.; Mendes, J.; Alves, O. L. *J. Nanoparticle Res.* **2006**, *8*, 141.
(12) Jenkins, R.; Snyder, R. L. *Introduction to X-ray Powder Diffractometry*; Wiley: New York, 1996.
(13) Richardson, J. T.; Yiagas, D. I.; Turk, B.; Forster, K.; Twigg, M. V. *J. Appl. Phys.* **1991**, *70*, 6977.
(14) Khadar, M. A.; Biju, V.; Inoue, A. *Mater. Res. Bull.* **2003**, *38*, 1341.
(15) Makhlouf, S. A.; Al-Attar, H.; Kodama, R. H. *Solid State Commun.* **2008**, *145*, 1.
(16) Smart, J.; Greenwald, S. *Phys. Rev.* **1951**, *82*, 1134.
(17) Alders, D.; Tjeng, L. H.; Voogt, F. C.; Hibma, T.; Sawatzky, G. A.; Chen, C. T.; Vogel, J.; Sacchi, M.; Iacobucci, S. *Phys. Rev. B* **1998**, *57*, 11623.
(18) Cangussu, D.; Nunes, W. C.; Corrêa, H. L. S.; Macedo, W. A. A.; Knobel, M.; Alves, O. L.; Souza Filho, A. G.; Mazali, I. O. *J. Appl. Phys.* **2009**, *105*, 013901.
(19) Nunes, W. C.; Socolovsky, L. M.; Denardin, J. C.; Cebollada, F.; Brandl, A. L.; Knobel, M. *Phys. Rev. B* **2005**, *72*, 212413.
(20) Mazali, I. O.; Alves, O. L. *J. Phys. Chem. Solids* **2005**, *66*, 37.
(21) Jagodic, M.; Jaglicic, Z.; Jelen, A.; Lee, J. B.; Kim, Y. M.; Kim, H. J.; Dolinsek, J. *J. Phys.: Condens. Matter* **2009**, *21*, 215302.
(22) Berkowitz, A. E.; Kodama, R. H.; Makhlouf, S. A.; Parker, F. T.; Spada, F. E.; McNiff, E. J., Jr.; Foner, S. *J. Magn. Magn. Mater.* **1999**, *196*, 591.
(23) Mydosh, J. A. *Spin-Glass: An Experimental Introduction*; Taylor and Francis: London, 1993.
(24) Nunes, W. C.; Folly, W. S. D.; Sinnecker, J. P.; Novak, M. A. *Phys. Rev. B* **2004**, *70*, 014419.
(25) Guo, S.; Liu, W.; Meng, H.; Liu, X. H.; Gong, W. J.; Han, Z.; Zhang, Z. D. *J. Alloys Compd.* **2010**, *497*, 10.
(26) Tiwari, S. D.; Rajeev, K. P. *Thin Solid Films* **2006**, *505*, 113.
(27) Thota, S.; Kumar, J. *J. Phys. Chem. Solids* **2007**, *68*, 1951.
(28) Berkowitz, A. E.; Takano, K. *J. Magn. Magn. Mater.* **1999**, *200*, 552.
(29) Madsen, D. E.; Mørup, S.; Hansen, M. F. *J. Magn. Magn. Mater.* **2006**, *305*, 95.

JP1046886